Gold Nanoparticles Capped with a Novel Titanium(IV)-Containing Polyoxomolybdate Cluster: Selective and Enhanced Bactericidal Effect Against *Escherichia coli*

Mónica Paesa, Fernando Almazán, Cristina Yus, Víctor Sebastián, Manuel Arruebo, Luis M. Gandía, Santiago Reinoso,* Ismael Pellejero,* and Gracia Mendoza*

Bacterial infections are a public health threat of increasing concern in medical care systems; hence, the search for novel strategies to lower the use of antibiotics and their harmful effects becomes imperative. Herein, the antimicrobial performance of four polyoxometalate (POM)-stabilized gold nanoparticles (Au@POM) against *Escherichia coli* (*E. coli*) and *Staphylococcus aureus* (*S. aureus*) as Gram-negative and Gram-positive bacteria models, respectively, is studied. The bactericidal studies performed, both in planktonic and sessile forms, evidence the antimicrobial potential of these hybrid nanostructures with selectivity toward Gram-negative species. In particular, the Au@GeMoTi composite with the novel $[Ti_2(HGeMo_7O_{28})_2]^{10-}$ POM capping ligand exhibits outstanding bactericidal efficiency with a minimum inhibitory concentration of just 3.12 μM for the *E. coli* strain, thus outperforming the other three Au@POM counterparts. GeMoTi represents the fourth example of a water-soluble Ti^{IV}-containing polyoxomolybdate, and among them, the first sandwich-type structure having heteroatoms in high-oxidation state. The evaluation of the bactericidal mechanisms of action points to the cell membrane hyperpolarization, disruption, and subsequent nucleotide leakage and the low cytotoxicity exerted on five different cell lines at antimicrobial doses demonstrates the antibiotic-like character. These studies highlight the successful design and development of a new POM-based nanomaterial able to eradicate Gram-negative bacteria without damaging mammalian cells.

1. Introduction

Polyoxometalates (POMs) are a large class of nanosized anionic metal-oxygen clusters with diverse molecular topologies in which controlled compositional modifications can be systematically performed at the atomic scale. This fact, together with their remarkable acid-base and redox properties, endows POMs with relevant potential applications in a range of fields including catalysis, energy, sensing, biomass valorization, electronics, or materials science.[1–6] Among their properties, the ability to act as electron and proton reversible reservoirs through fast redox processes of multi-step nature while keeping their structure nearly intact stands out. It is well known that UV light can promote such proton-coupled redox processes, and thus, POMs emerge as ideal carriers for the photosynthesis of monodispersed metal nanoparticles (NPs), playing a dual role as reducing agents and stabilizers. POMs mediate the electron transfer from a sacrificial donor (typically alcohols or amines) to the metal ions and, once the resulting metallic nanostructures are formed, they form a protective shell

M. Paesa, C. Yus, V. Sebastián, M. Arruebo
Instituto de Nanociencia y Materiales de Aragón (INMA)
CSIC-Universidad de Zaragoza
Zaragoza 50009, Spain

M. Paesa, C. Yus, V. Sebastián, M. Arruebo
Department of Chemical Engineering
University of Zaragoza
Campus Río Ebro-Edificio I+D, C/Poeta Mariano Esquillor S/N, Zaragoza 50018, Spain

F. Almazán, L. M. Gandía, S. Reinoso, I. Pellejero
Instituto de Materiales Avanzados y Matemáticas (INAMAT2)
Universidad Pública de Navarra (UPNA)
Edificio Jerónimo de Ayanz
Campus de Arrosadia
Pamplona 31006, Spain
E-mail: santiago.reinoso@unavarra.es; ismael.pellejero@unavarra.es

enclosing the metal core that inhibits further agglomeration. In contrast to the most common protective ligands (e.g., carboxylates, phosphates), POM-stabilized metal NPs exhibit boosted and synergistic performance compared to pristine POMs,[7] thereby increasing the applicability in heterogeneous catalysis, liquid-phase oxidation, sensors or energy storage, among other disciplines.[8,9]

The biomedical aspects of POMs have become increasingly encouraging over the past years as the features affecting their interaction with biological targets may be customized for given specific applications.[10,11] Their rigid structures and bioactivity provide unique characteristics that have been found relevant in different fields such as anticancer, antiviral, and antimicrobial therapies.[12–14] The biological activity of POMs commonly results from their electrostatic interaction with proteins aided by hydrogen bonding. The negatively charged clusters are mainly found within or at positively charged protein regions,[11,15] though covalent interactions between POMs and biomacromolecules have also been demonstrated.[16]

The search for new strategies against microbial infections is imperative to fulfill two basic requirements: to behave as an antibiotic by eradicating bacteria cells without damaging mammalian cells and to avoid the generation of resistances. Traditional antibiotics exert their bactericidal action through the invasion of bacterial cells and the attack against the bacterial membrane or specific molecular targets. This action, in some cases, does not mainly yield substantial physical damage in the cell membrane and/or wall, which may result in the development of resistances with the concomitant threat to public health.[17–20] In this regard, POM-based antimicrobial strategies have been proposed in recent years as a promising approach to face the serious threat of bacterial infections to human, environmental, and animal health.

Polyoxotungstates (POTs), -vanadates (POVs), and -molybdates (POMos) have all been widely assayed and shown promising bactericidal ability against different Gram-positive and Gram-negative bacteria strains. These studies point to higher efficiency of POTs and POVs against Gram-positive bacteria, and POMos against Gram-negative bacteria.[21–24] Moreover, the use of UV[23] or NIR[25] light irradiation has been shown as a potent booster to enhance the bactericidal action of POMos and POTs, ascribing these improved antimicrobial and antibiofilm activities to the oxidizing properties of excited POMs throughout ROS (reactive oxygen species) generation. Interestingly, the combination of POMs with traditional antibiotics (e.g., streptomycin, oxacillin, and spectinomycin) has also been reported as a relevant strategy against resistances because it allows for achieving higher antimicrobial efficiency at lower antibiotic doses mediated by the POM activity.[21,22,26] The bactericidal mechanism of POMs has been proposed to be based on their interaction with some of the biomacromolecules present in bacteria surfaces. Among other enzymes, phosphatases, ecto-nucleotidases, and transferases are found in bacteria walls or membranes and POMs may interact with such enzymes to result in the disruption of intracellular metabolic pathways and consequent bacteria death.[12]

In this context, the search for novel POM architectures that can exert enhanced antibiotic activity without generating resistances emerges as an attractive scientific challenge. For POTs, the most widely used approach to accomplish such a goal consists in the combination of 3d- and/or 4f-metal ions with lacunary POMs acting as polydentate O-donor ligands thanks to displaying *addenda*-metal vacant sites in the cluster skeleton. This strategy has resulted in a vast library of transition metal (TM)-substituted heteroPOT families,[27–29] among which Ti^{IV}-containing species have shown promising bioactivity.[30,31] In particular, the long-known Ti^{IV}-disubstituted $[PTi_2W_{10}O_{40}]^{7-}$ Keggin-type anion (PWTi)[32] has been found to display broad-spectrum antiviral activity (herpes simplex, hepatitis B, RNA viruses)[33–35] and to enhance β-lactam antibiotics against multiresistant *Staphylococcus aureus* (*S. aureus*) strains.[36,37] The landscape becomes completely different when looking at TM-substituted heteroPOMos. The use of lacunary POMo ligands is limited because of their high instability in solution and their kinetically fast rearrangement reactions,[38] which results in the current catalog of TM-substituted heteroPOMos being short and much underdeveloped compared to their heteroPOT counterparts.[39] Focusing on Ti^{IV}-containing species, the literature affords only three water-soluble examples to our knowledge: the $[\{PMo_9O_{34}TiO\}_2]^{14-}$ dimer[40] and two sandwich-type anions with general formula $[Ti_2(X^{III}Mo_7O_{27})_2]^{10-}$ (X^{III} = Sb, As).[41] Studies on the potential bioapplications of these POMs have not been reported yet.

Our work aims at developing new POM-based antimicrobial strategies to eradicate bacterial infections while being harmless to mammalian cells, thus exerting antibiotic features while preventing the generation of resistances. To this end, we look for synergistic effects between colloidal metallic NPs and unprecedented POM assemblies as functional capping agents and provide the possible mechanisms of action for their bactericidal ability. Herein, we report i) the novel $[Ti_2(HGeMo_7O_{28})_2]^{10-}$ (GeMoTi) cluster as the fourth water-soluble Ti^{IV}-containing heteroPOMo known to date; ii) its use as stabilizing ligand for the photo-assisted preparation of monodispersed metallic gold nanoparticles (Au@GeMoTi); and iii) the antimicrobial activity of the latter hybrid nanostructures against *Escherichia coli* (*E. coli*) as a model of Gram-negative bacteria and *S. aureus* as Gram-positive bacteria, both in planktonic cultures and as sessile (i.e., biofilm-forming) forms. The potential bactericidal mechanisms are also studied, as well as the cytotoxic effects of the treatment with such NPs on mammalian cells. For comparative purposes, analogous tests are performed for an additional Au@POM set with three other known POMs: the above-mentioned PWTi, for which

F. Almazán, L. M. Gandía, S. Reinoso, I. Pellejero
Departamento de Ciencias
Universidad Pública de Navarra (UPNA)
Edificio los Acebos
Campus de Arrosadia
Pamplona 31006, Spain
V. Sebastián, M. Arruebo, G. Mendoza
Aragon Health Research Institute (IIS Aragon)
Zaragoza 50009, Spain
E-mail: gmendoza@iisaragon.es
V. Sebastián, M. Arruebo, G. Mendoza
Networking Research Center on Bioengineering
Biomaterials and Nanomedicine
CIBER-BBN
Madrid 28029, Spain

2305169 (2 of 13)

ADVANCED
SCIENCE NEWS

www.advancedsciencenews.com

NANO · MICRO
small
www.small-journal.com

POM-stabilized gold NPs have not been reported yet, and the commercial $H_3PW_{12}O_{40}$ (PW) and $H_3PMo_{12}O_{40}$ (PMo) heteropolyacids.

2. Results and Discussion

2.1. The POM Precursor GeMoTi

To enlarge the limited collection of TM-substituted heteroPOMos with additional Ti^{IV}-containing species, we undertook a combinatorial approach to one-pot syntheses starting from three different heteroatomic sources (GeO_2, Na_2HPO_4, Na_2SiO_3), two different Mo precursors (Na_2MoO_4, $(NH_4)_6Mo_7O_{24}$) and a single Ti reagent ($TiOSO_4$). The reactions were carried out in different aqueous media (water, aqueous alkali metal chloride solutions, acetate buffers) either at room temperature or 90 °C and at pH values ranging from 6.0 to 1.0. Out of these systematic studies, the new POM GeMoTi was isolated as the sodium salt $Na_{10}[Ti_2(HGeMo_7O_{28})_2]\cdot34H_2O$ in moderate-to-good yields from the synthesis GeO_2:Na_2MoO_4:$TiOSO_4$ (1:9:2.2 molar ratio) in aqueous 0.5 M sodium acetate buffer (pH 4.7) regardless of the reaction temperature (see Figures S1 and S2, Supporting Information, for routine characterizations).

Single-crystal XRD analysis shows that the molecular structure of GeMoTi consists of a central $\{Ti_2O_{10}\}$ core of two edge-sharing TiO_6 octahedra sandwiched in ideal C_{2h} symmetry by two MoO_2-monocapped Keggin-type $\{HGeMo_7O_{28}\}$ hexalacunary subunits (**Figure 1**a). These subunits belong to the B-form and can be formally derived from the corresponding plenary Keggin cluster by removing two edge-sharing $\{Mo_3O_{13}\}$ trimers, the additional $\{MoO_2\}^{2+}$ capping moiety grafting at the single remaining $\{Mo_4O_{16}\}$ tetrameric face (Figure S3a, Supporting Information). They constitute a new structural feature in POMo chemistry as analogs have only been observed with lone-pair containing heteroatoms (As^{III}, Sb^{III}) instead of Ge^{IV}, leading to subunits with general formula $\{XMo_7O_{27}\}$ instead of $\{XMo_7O_{28}\}$.[41–43]

The sandwich-type structure of GeMoTi closely resembles that of the previously reported $[Ti_2(X^{III}Mo_7O_{27})_2]^{10-}$ (X^{III} = Sb, As) anions[41] (Figure S3b, Supporting Information). This type of architecture was initially described for $[TM_2(AsMo_7O_{27})_2]^{n-}$ assemblies[42,43] with central cores made of TM = Cu^{II}, Fe^{III}, Cr^{III}, thus constituting a structural archetype for TM-substituted POMos with lone-pair containing heteroatoms where a variety of TM ions from divalent to tetravalent can function as the core atoms. The isolation of GeMoTi represents the first evidence of such an archetype being also achievable with heteroatoms in high-oxidation states, which marks a key difference in its potential use as a capping ligand. In all cases, two out of the six metal vacant sites on each hexalacunary subunit are saturated by the Ti atoms, leading to POM fragments related to the Keggin-type trilacunary B-β-isomer with the $\{Ti_2O_{10}\}$ core in place of the 60°-rotated trimer (Figure S3c, Supporting Information). The shape of the $\{GeTi_2Mo_7O_{33}\}$ fragment in GeMoTi is not unusual in heteroPOMo chemistry, but has always been observed without TM-substitution as in some $[TM_2(XMo_9O_{33})_2]^{n-}$ examples.[44,45] The remaining vacant sites in the archetype are blocked for $[TM_2(X^{III}Mo_7O_{27})_2]^{n-}$ assemblies due to the steric hindrance exerted by the heteroatomic lone-pair, but this is replaced in GeMoTi with a terminal Ge—OH group (O protonation
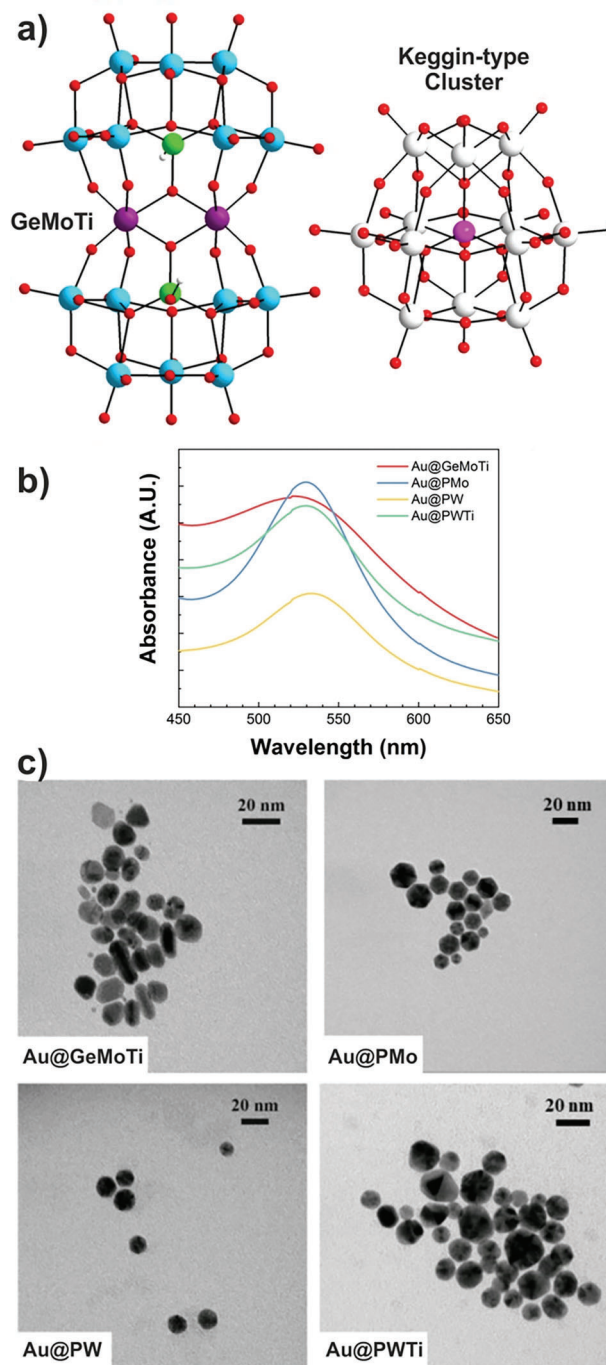

Figure 1. a) Molecular structure of GeMoTi (color code: Mo, blue; Ge, green; Ti, violet; O, red) compared to the $\{\alpha\text{-}XM_{12}O_{40}\}$ Keggin-type cluster (X, pink; M, light gray). b) UV–vis spectra and c) TEM images of the Au@POM nanostructures synthesized in this work.

confirmed by a Bond Valence Sum[46] of 1.269), making those sites potentially available for saturation with additional metals. Close inspection of the crystal packing reveals indeed two sodium ions incorporated at those positions (Figure S3d, Supporting Information), which supports the availability of vacant sites for further metal coordination in GeMoTi.

**ADVANCED
SCIENCE NEWS**

www.advancedsciencenews.com

**NANO · MICRO
small**

www.small-journal.com

The sample used for single-crystal XRD is illustrative of the bulk GeMoTi material, as demonstrated by the good reliability factors derived from the full-profile matching of the powder XRD pattern to a monoclinic $P2_1/c$ phase (Figure S4, Supporting Information). The lattice parameters afforded by this pattern-matching analysis agree with those obtained at 100 K by single-crystal XRD, thereby confirming bulk GeMoTi as a homogeneous crystalline phase. The solution stability of GeMoTi in water was assessed by UV–vis spectroscopy. The spectrum of a freshly prepared 0.7 mM sample is dominated by two absorption maxima at 230 and 245 nm accompanied with a broad signal centered at 210 nm and remains unmodified when compared to that of a stock solution aged for 1 month (Figure S5, Supporting Information), thus showing that GeMoTi is stable upon dissolution and does not undergo any structural rearrangement or side reaction for weeks. The solution stability under UV light was also investigated by irradiating the above sample with a 365 nm LED lamp in the presence of isopropyl alcohol (IPA) as a sacrificial electron donor, its color darkening to deep blue due to the Mo^{VI} to Mo^V reduction as shown by the appearance of an additional absorption at 715 nm (Figure S6, Supporting Information). The intensity increase of such absorption was monitored for 1 h and the final blue photolyte was left to oxidize while evaporating in an open vessel to dryness. The FT-IR spectrum of the resulting pale-yellow solid, as well as its powder XRD pattern, were virtually identical to those of GeMoTi. This result evidences that GeMoTi can undergo reversible redox processes without any structural impact (Figure S6, Supporting Information). The combination of possessing vacant skeletal sites available for metal coordination with the solution stability shown under UV light makes GeMoTi a suitable capping ligand for the preparation of POM-stabilized metal NPs.

2.2. Au@POM Hybrid Nanostructures

The synthesis of hybrid Au@GeMoTi nanoparticles was carried out through an adaptation of Troupis and Papaconstantinou's method,[47] previously used in our group to prepare Au@POM nanostructures for catalytic or SERS-sensing purposes.[9,48] This method consists of the POM-assisted photoreduction of the gold precursor $HAuCl_4$ in aqueous 0.5 M IPA, thus using IPA as a sacrificial electron donor. In this process, the POM has three main roles: i) to mediate the electron transfer from the sacrificial donor to the Au^{III} centers through photoinduced redox cycles, ii) to stabilize the so formed Au^0 metal cores by self-assembling in a protective monolayer iii) to prevent agglomeration thanks to the outer POM shells undergoing electrostatic repulsion.

To avoid the use of short-chain alcohols undesirable in antimicrobial studies, IPA was in this work replaced with the long-chain, water-soluble, and biocompatible polyvinyl alcohol (PVA). The interaction of PVA chains and POMs has been reported to benefit the bactericidal properties due to the PVA coating effect enhancing the POM thermo-oxidative stability, as observed for $PVA/PEI-H_5PV_2Mo_{10}O$ nanohybrid membranes with strong antibacterial activity against both Gram-negative and Gram-positive bacteria.[49] To this end, the photo-induced synthetic protocol above was slightly modified (see Experimental Section) upon a thorough study of the reaction conditions (precursor concentra-

tions, PVA addition – solid versus solution -, irradiation time and light irradiance) that was preliminarily carried out (not shown here) in order to assure complete Au^{III} reduction and to maximize the Au^0 concentration in the final solution, but avoiding precipitation of aggregated NPs or brown Au^0 colloids at the same time. Compared to our previous IPA-based syntheses,[9,48] the use of a PVA as an electron donor allowed us to scale the POM concentration up by almost 3 times, but it significantly increased the irradiation time needed instead. The reaction solution darkened from yellow to burgundy color after 1 h of stirring under UV irradiation confirming substantial Au@GeMoTi formation, but according to the UV–vis monitorization of the intensity of the surface plasmonic resonance absorption (Figure S7, Supporting Information), it had to be kept under UV light for an additional 1 h for the signal to reach saturation, thereby assuring a complete gold reduction. The redox activity of Au@GeMoTi nanoparticles under UV-LED irradiation was also monitored in buffered PBS medium at different time points and a significant development of singlet oxygen production was observed with increasing the irradiation time. These mechanisms could be of relevance in the bactericidal effects of Au@GeMoTi.

For comparative purposes, an additional Au@POM set was also prepared following the same protocol but using three other well-known POM photocatalysts: PWTi ($[PTi_2W_{10}O_{40}]^{7-}$), widely considered as a reference standard for Ti^{IV}-substituted POMs, and the commercial PW ($H_3PW_{12}O_{40}$) and PMo ($H_3PMo_{12}O_{40}$) heteropolyacids. All of them show the typical structure of the α-Keggin archetype depicted in Figure 1a. These three POM species were selected to investigate how the Au@POM bactericidal performance can be affected by modifications in the POM skeleton, such as the type of addenda metal (Mo^{VI}, Ti^{IV}, and W^{VI}), the heteroatom (Ge^{IV} vs P^V) or the molecular topology (elongated with vacant sites versus plenary globular).

The characterization of the four types of plasmonic Au@POM hybrid nanostructures used in this work by UV–vis spectroscopy and TEM is shown in Figure 1b,c, respectively. The UV–vis spectra display intense surface plasmonic resonance absorption maxima at 523 nm for GeMoTi, 530 nm for PMo, 529 nm for PWTi, and 531 nm for PW. The TEM image analyses revealed homogeneous colloids of monodispersed nanostructures with nearly spherical shape for the four Au@POM samples and afforded comparable average sizes in all cases, the diameters being ≈10.4 ± 4.5, 31.9 ± 9.1, 18.3 ± 9.8, and 13.5 ± 3.5 nm for Au@GeMoTi, Au@PMo, Au@PWTi, and Au@PW, respectively. Compared to our previous IPA-based NPs,[9,48] the plasmon resonances of the Au@POM nanohybrids in this work are slightly blueshifted, the particle sizes are noticeably smaller, and the size-distribution dispersions are somewhat narrower. These results might originate from the fact that PVA slowly dissolved during the irradiation time, thus providing a controlled release of the sacrificial electron donor for precise Au^{III} reduction that decreased the formation speed of Au^0 nuclei. These nuclei could then be fast capped by the POM clusters present in high concentration, thereby preventing further growth and leading to homogeneous, small-sized Au@POM nanostructures. The PVA present in the reaction medium is also expected to act as a coating agent, helping to stabilize the colloidal dispersions[50] by avoiding the precipitation of aggregated Au@POM nanostructures even at the high Au:POM concentrations used in this work (up to 1 mM). Our NP
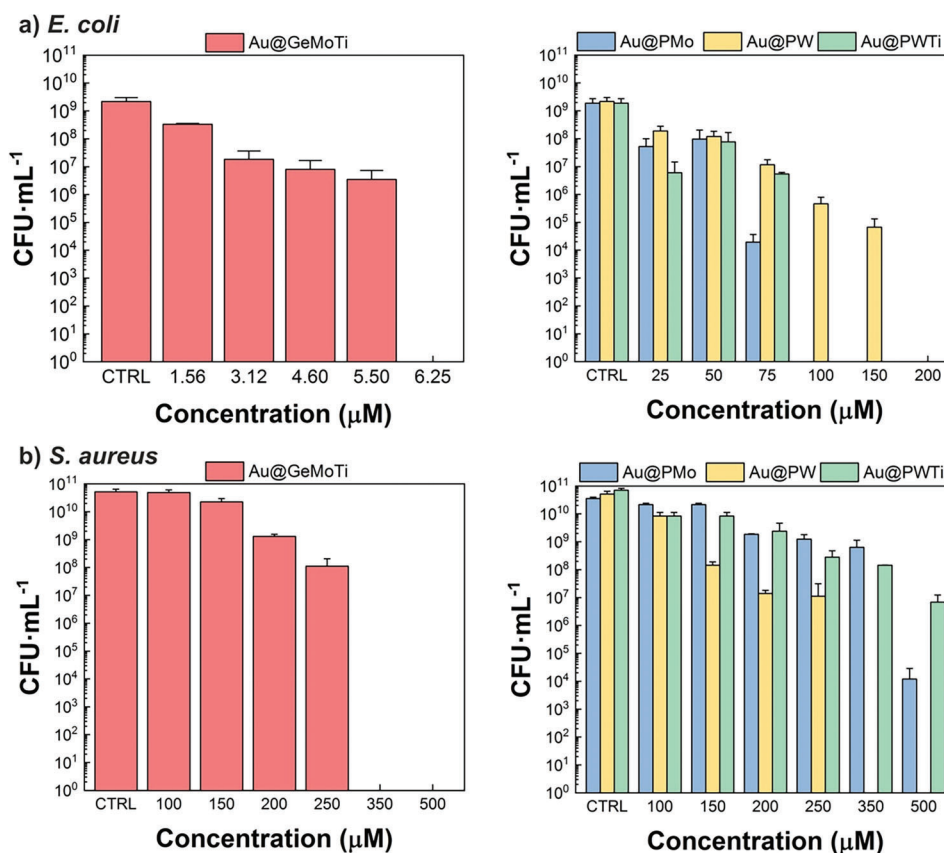
**ADVANCED
SCIENCE NEWS**

www.advancedsciencenews.com

**NANO · MICRO
small**

www.small-journal.com

Figure 2. Bacteria growth (CFU mL^{-1}) after treatment with Au@POM samples (0–500 μM) for 24 h: a) *E. coli*. b) *S. aureus*. Control samples represent bacteria cultures not treated with Au@POM nanoparticles but adding PVA amounts equal to those present in the highest Au@POM concentration assayed. At least three experiments in triplicate were used to represent mean ± SD.

solutions displayed outstanding stability, as they remained virtually the same even after storage for more than one year at 4 °C (results not shown).

2.3. Bactericidal Activity of Au@POM Nanoparticles

The antibacterial activity of the four types of as-prepared Au@POM nanostructures (Au@GeMoTi, Au@PMo, Au@PW, and Au@PWTi) in *E. coli* and *S. aureus* cultures is depicted in **Figure 2**. The Au@POM addition to *E. coli* cultures inhibited the bacteria growth significantly (Figure 2a), showing minimum inhibitory concentration (MIC) values in the 3.12–75 μM range. Au@GeMoTi was the most effective inhibitor, showing the lowest MIC (3.12 μM) among all samples tested (≈20 times lower). Previous studies in *E. coli* cultures have reported PMo to exhibit lower MIC values than PW, which could be related to its superior chemical stability and redox properties.[22,23,51] These results point to POM stability as a significant feature of their biological activity. Other authors have also studied the effect of POTs on Gram-negative bacteria cultures, showing MIC values in the range of ours (125–330 μg mL^{-1}).[24,52] Interestingly, an Au@GeMoTi concentration of only 3.12 μM (0.614 μg$_{Au}$ mL^{-1} and 7.744 μg$_{GeMoTi}$ mL^{-1} for the cluster without counterions) was enough to significantly inhibit the bacteria growth, whereas no

growth (minimum bactericidal concentration, MBC) was found when *E. coli* was treated with a concentration of 6.25 μM. The bactericidal effect of Au@GeMoTi is comparable to that of some pharmaceutical antibiotics (see Table S1, Supporting Information) and superior to other Au NPs synthesized using well-known stabilizing agents like citrate[53] or polysaccharides.[54] It is also superior to that found for diverse POM hybrid materials, such as PMo-graphene oxide[55] or PW-peptide conjugates.[52]

In *S. aureus* cultures (Figure 2b), the Au@POM treatments were also effective in inhibiting the bacteria growth, but at concentrations significantly higher than those achieved in *E. coli* (150–500 μM). Zhang et al.[56] found that the MIC for *S. aureus* ATCC29213 was 32 μg mL^{-1} when adding a nanocomposite including PW and Ag instead of Au, which may be the reason for the lower concentration to inhibit the bacteria growth compared to our results for Au@PW and Au@PWTi (25–500 μM). Gram-negative and Gram-positive bacteria differ in their cell wall structure. The former possesses an outer multilayered membrane, which serves as a selective permeability barrier avoiding the penetration of foreign molecules, whereas the latter presents a thick single-layer peptidoglycan cell wall. These structures involve differences in their protection against antimicrobial drugs.[23,51]

In order to explore whether our Au@POM nanoparticles exhibit any additive or synergistic bactericidal effect between POM

**ADVANCED
SCIENCE NEWS**

www.advancedsciencenews.com

**NANO · MICRO
small**

www.small-journal.com

ligands and Au^0 metal cores in comparison to pristine POM clusters, additional inhibitory and bactericidal concentration assays were conducted in *E. coli* samples following the same protocol above but using POM solutions with concentrations in the same ranges as those of the Au@POM samples (Figure S8, Supporting Information). Compared to bacteria control samples, no inhibition of bacteria growth was observed in this case for the concentration ranges tested, highlighting relevant synergism between the components of our hybrid Au@POM nanostructures that allow for achieving antimicrobial effect. Similar results were found for hybrid Tyrosine-capped Ag-$H_3PW_{12}O_{40}$ and Ag-$H_3PMo_{12}O_{40}$ NP systems, in which neither of the two pristine POMs exhibited antibacterial activity when tested alone.[57] Neither this core-coating synergistic effect nor any observation of bacteria inhibition is present when Au NPs are coated and stabilized with non-active capping ligands like citrate,[53] PVA,[58] or PEG[59] (polyethylene glycol). However, we have recently shown that Au^{III} solutions are able to induce bacterial wall damage, being much more harmful against Gram-negative than Gram-positive bacteria.[60] This previous study demonstrated the biosynthetic generation of Au NPs by bacteria after treatment with gold ionic species, and proteomics and genomics showed the molecular mechanisms responsible for gold toxicity against Gram-negative bacteria.

Considering the superior bactericidal performance displayed by Au@GeMoTi, we further aimed to evaluate the influence of UV-light irradiation on its inhibiting activity toward bacteria growth (Figure S9, Supporting Information). Irradiated Au@GeMoTi solutions (365 nm LED, 1350 mW, 1 h) were assayed in *E. coli* cultures and no growth was observed neither after 20 min of irradiation at MIC value, nor after 15 min of treatment at 10 times the MIC. Irradiation significantly increased the Au@GeMoTi antimicrobial activity, achieving the MBC in only 20 min of incubation with the MIC determined for the non-irradiated samples. This may be attributed to the significant increase in singlet oxygen production after LED irradiation mentioned above (Figure S7, Supporting Information). Moreover, the bactericidal ability of GeMoTi alone was also tested at the same conditions. However, the bacteria growth was in the range of control samples (Figure S9, Supporting Information), pointing to the synergistic relationship between the Au core and the GeMoTi ligands as key to developing antimicrobial effects. Control samples in which Au@GeMoTi or UV light was absent did not show *E. coli* growth inhibition (results not shown). Hybrid Au@GeMoTi nanostructures could interact and penetrate the cell membrane of Gram-negative bacteria, as other researchers have demonstrated with Keggin-type POTs,[22] and may then activate oxidation processes inside the cells upon irradiation with UV light, leading to cell damage and enhancing the bactericidal activity.[23]

Synergistic interactions between Au@GeMoTi and the three other Au@POM nanostructures assayed were also investigated. Fractional Inhibitory Concentration Index (FICI) values obtained against *E. coli* (Table S2 and Figure S10, Supporting Information) indicate that the combination of Au@GeMoTi and Au@PW has a synergistic effect, whereas an additive effect is found with Au@PWTi. No interaction between Au@GeMoTi and Au@PMo nanoparticles was retrieved. These results might be attributed to the different specific metal compositions in each Au@POM

nanostructure and we plan to develop further studies in the near future to ascertain this hypothesis.

2.4. Antimicrobial Mechanisms of Au@POM Nanoparticles

To assess the antimicrobial mechanism exerted by our Au@POM nanostructures, the bacteria morphology, membrane polarization, and nucleic acid release were evaluated. The morphological changes on bacteria observed by SEM before (control sample) and after Au@POM treatment at MIC values, either irradiated at 365 nm or non-irradiated, are depicted in **Figure 3**a (*E. coli*) and Figure S11a (Supporting Information) (*S. aureus*).

The images show clear damage inflicted by Au@POM nanoparticles in the bacteria walls or outer membranes regardless of whether the samples are irradiated or not. Both *E. coli* and *S. aureus* show an increase in size and surface roughness, disrupted surface, and loss of morphology, pointing to cell wall or membrane damage as the Au@POM bactericidal mechanism. Before the bacteria's death, cell filamentation, and elongation result from the alteration in cell size and shape under oxidative stress due to the bacteria's response against external damage by growing without any cell division.[52] Differences in the bacteria morphology between irradiated and non-irradiated samples are not found in any case. As depicted in the micrographs, nanostructures with Keggin-type POMs are observed to be adhered to the bacteria wall or membrane, which agrees with previous studies regarding Gram-negative bacteria.[24] In contrast, no Au@GeMoTi clustering on the bacteria surface is observed, probably because of its large aqueous solubility and colloidal stability even in culture media.

The membrane disintegration feature of bacterial cells was confirmed via flow cytometry analysis by quantifying changes in the membrane potential (Figure 3a for *E. coli*; Figure S11b, Supporting Information, for *S. aureus*). The hyperpolarization of the cell membrane represents changes within cells, in particular a variation in the distribution of the electrical charge associated with the intracellular exchange of cations and anions, resulting in a lower negative charge in the cell. Some bacteria have demonstrated the ability to modulate this ion flux to counteract the impact of different antibiotics. Thus, the design of novel NPs able to interact with the bacteria membrane and hamper the ion flux would be very promising for the treatment of bacterial infections.[26] After 2 h of incubation with Au@POM samples at MIC and MBC values, the percentages of hyperpolarized cells slightly increased (<10%) compared to the control ones for all nanostructures except Au@GeMoTi, for which the percentage was remarkably higher reaching almost 90%. After 24 h of incubation at MIC values, the percentage of hyperpolarized cells significantly increased in all Au@POMs tested, being more pronounced for the molybdenum-based Au@PMo and Au@GeMoTi hybrids as their larger shift in both forward and side scatter characteristics reveal (complexity and size, see Figure S11b, Supporting Information). It is known that PO-Mos are more prone to reduce than POT analogs,[61] and therefore, the presence of molybdenum could correlate with a higher oxidizing strength, which may lead to a superior antibacterial activity in turn. This interpretation is supported by previous
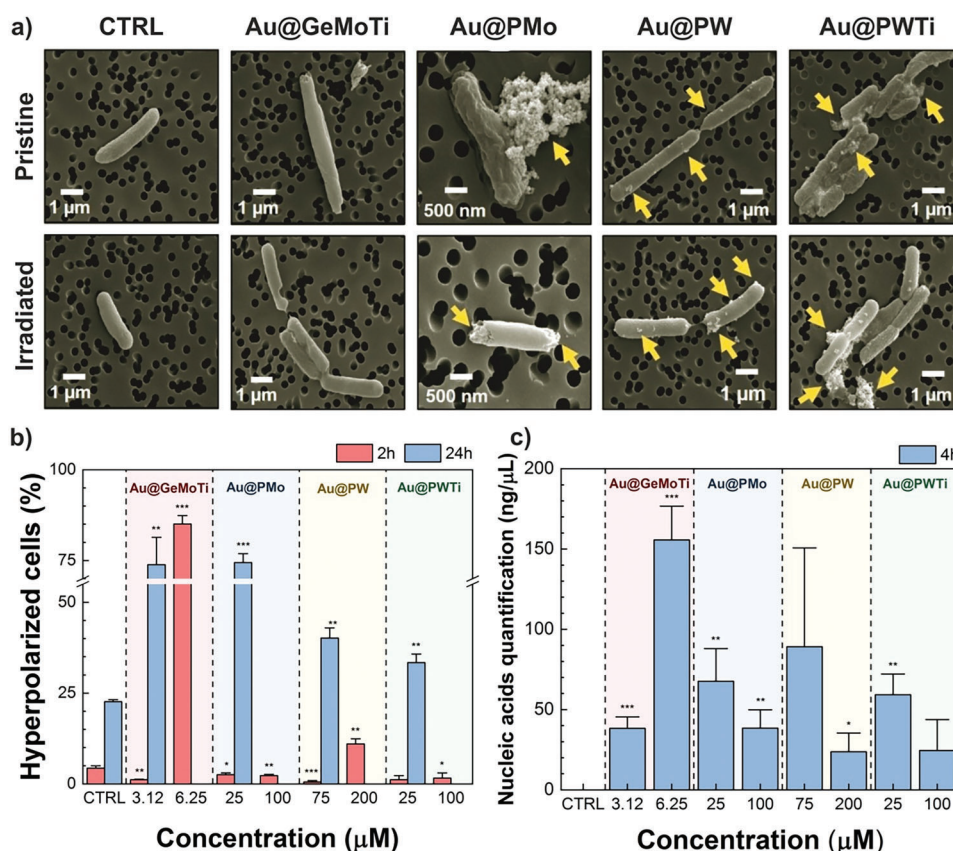
**ADVANCED
SCIENCE NEWS**
www.advancedsciencenews.com

**NANO · MICRO
small**
www.small-journal.com

Figure 3. Au@POM antimicrobial mechanisms against *E. coli*: a) SEM images of pristine and UV-irradiated *E. coli* bacteria before (control) and after incubation with Au@POM samples for 24 h at MIC values (arrows indicate the location of representative Au@POM nanostructures on the bacteria). b) Quantitative measurement by flow cytometry of the bacteria membrane potential after Au@POM treatment at MIC and MBC values for 2 and 24 h. c) Quantification of the bacteria nucleic acid release after incubation with Au@POM samples at different concentrations for 4 h. Results were normalized to the control. Data are expressed as mean ± SD of at least three independent experiments performed in triplicate. Statistically significant differences between control and treated samples: $^*p < 0.05$; $^{**}p < 0.01$; $^{***}p < 0.001$; and $^{****}p < 0.0001$.

studies that have demonstrated higher antimicrobial activity of alendronate-POV capped NPs@POV^V gold NPs compared to citrate capped CitNPs@POV$^{IV}_{red}$ analogs against *S. epidermidis* due to the oxidation state of the vanadium centers.[62] In this line, Li and coworkers have shown that the copper-containing hybrid [{Cu(phen)$_2$}$_2$(H$_4$W$_{12}$O$_{40}$)] exerts higher antibacterial activity, pointing to the importance of the elemental composition rather than the molecular structure itself.[63] These results are in accordance with our SEM images showing the Au@POM ability to disrupt the cell membrane integrity. Similar results were obtained with [MP$_5$W$_{30}$O$_{110}$]$^{14-}$ Preyssler-type POMs (M = Na, Ag),[26] with a [Co(L)$_2$]$_3$[PMo$_{12}$O$_{40}$] hybrid combining a Keggin-type POM and thiosemicarbazones,[51] and with peptide-based polymer-POM composites,[52,64,65] which are all able to modulate the cell growth rate of bacteria by modifying the membrane potential.

The nucleic acid release after incubation of *E. coli* with Au@POM samples was also evaluated (Figure 3c; Figure S11c, Supporting Information) as cell wall or membrane damage may involve the release of cytoplasmic components to the culture medium. The evaluation of the released nucleic acids was carried out by measuring the fluorescence signal detected by the

Qubit™ ssDNA Assay kit, as well as by flow cytometry mediated by propidium iodide. No released nucleic acids were detected after 2 h of Au@POM treatment of *E. coli* cultures at concentrations in the range of MIC and MBC; the obtained data fell in the range of control samples (non-treated bacteria; data not shown). However, a significant detection was achieved after 4 h (Figure 3c), being more pronounced at the highest Au@GeMoTi concentration assayed (6.25 μM). These results were confirmed by flow cytometry in which only nucleic acids from dead bacteria or with damaged membranes were stained by propidium iodide, observing the highest signal (>40%) after 24 h of treatment with Au@GeMoTi and Au@PW (Figure S11c, Supporting Information). This may imply that cell lysis and nucleic acid release began in *E. coli* after 4 h of Au@POM treatment, being more pronounced for Au@GeMoTi. Leakage of intracellular components and loss of cell integrity have been previously reported after treatment with AgPW@PDA@Nisin nanoflowers,[56] as well as with the above-mentioned POV-capped NPs@POV nanoparticles[62] and the [Co(L)$_2$]$_3$[PMo$_{12}$O$_{40}$] hybrid.[51] These data agree with the SEM images and the changes in the bacteria membrane polarization (Figure 3; Figure S11, Supporting Information), confirming that our Au@POM nanostructures can also cause irreversible
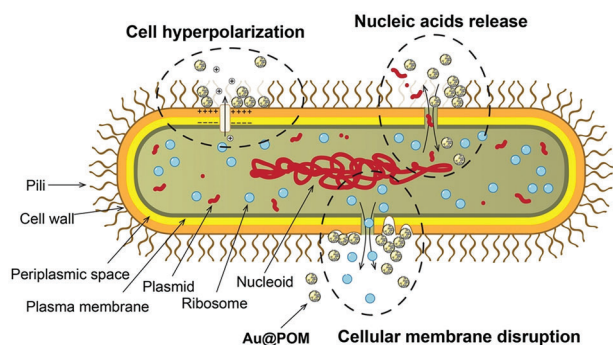
Figure 4. Schematic overview of the putative mechanisms of antibacterial Au@POM systems: Au@POM targets include Cell hyperpolarization, Nucleic acids release, and Cellular membrane disruption.

bacterial cell damage, intracellular material leakage, and eventual cell death.[17,63,66]

Figure 4 schematizes the putative Au@POM mechanisms of action. In brief, Au@POM nanohybrids are able to strongly adhere to cell membranes, which results in the hyperpolarization of the bacterial cells with subsequent membrane cell wall disruption and leakage of intracellular moieties. All of these damages consequently lead to bacteria cell death.

2.5. Disruption of *E. coli* Biofilms by Au@POM Nanoparticles

Biofilms produced because of antibiotic overuse have emerged as a health threat worldwide, being the main cause of antimicrobial therapy failures. The higher resistance of biofilms is associated with their ability to elude phagocyte-initiated innate immune responses, as well as with the inhibition of antibiotic penetration through the thick exopolysaccharide matrix. Therefore, the search for novel antibacterial and antibiofilm strategies is urgently needed.[25,62] In this work, the capacity of Au@GeMoTi and irradiated-Au@GeMoTi samples to avoid biofilm formation and to disrupt an existing mature *E. coli* biofilm was explored following three distinct methodologies: i) the crystal-violet (CV) staining method, ii) the bacteria quantification by the microdilution method (CFU/mL), and iii) confocal microscopy (**Figure 5**; Figure S12, Supporting Information). The addition of Au@GeMoTi to bacteria suspensions prior to the biofilm formation inhibited this process up to 80% at all concentrations tested (3.12–25 μм), whereas a biomass reduction of 60–70% compared to the controls (100% biomass) was reached in preformed mature biofilms (Figure 5a). However, lower differences were found in the quantification method when compared to untreated biofilms, indicating that Au@POM concentration values higher than those of MIC and even MBC may be needed for bacteria eradication. According to the results obtained in both planktonic bacteria and sessile forms, an Au@GeMoTi concentration of 31.25 μм (10 times the MIC) was chosen for the subsequent experiments.

As shown in the confocal microscopy images in Figure 5b, the addition of Au@GeMoTi at 31.25 μм before and after the biofilm was formed clearly decreased the amount of biofilm (blue) and bacteria (red). The biofilm blue staining in the inhibition experiment is not very strong because *E. coli* being a sessile bacteria does not rapidly form a thick adherent biofilm, but a biofilm in

the air-liquid interface. However, the blue staining was clearly observed in the experiments on mature biofilm after 24 h. These results highlight the ability of Au@GeMoTi to prevent or eliminate *E. coli* biofilms. When Au@GeMoTi samples were preliminarily irradiated with UV light for 1 h and subsequently added to the bacteria suspension before and after the biofilm formation, reductions up to 80% and 30% were reached, respectively, in accordance with confocal images (Figure S12, Supporting Information). Interestingly, a reduction of the bacteria growth in two orders of magnitude was observed after the addition of irradiated-Au@GeMoTi to bacteria suspensions before biofilm formation, indicating its superior ability to eradicate bacteria and inhibit biofilm formation (Figure S12, Supporting Information). In this line, Zhang et al. showed that the combination of reduced-GdW$_{10}$O$_{36}$ clusters with NIR irradiation or/and H$_2$O$_2$ treatment efficiently enhances the antibacterial activity in *E. coli* and *S. aureus* biofilms with a clear reduction of biomass formation and thickness.[25]

2.6. Cytocompatibility of Au@POM Nanoparticles

Considering that the evaluation of the mammalian cell cytotoxicity is an essential indicator for antimicrobial applications, our four types of Au@POM nanohybrids were evaluated in five cell lines: fibroblasts, keratinocytes, macrophages, mouse mesenchymal stem cells (mMSCs) and U251MG cell lines (**Figure 6**). Cells were treated for 24 h at different concentrations in the 100–250 μм range corresponding to the MIC and MBC values obtained from *E. coli* and *S. aureus* planktonic cultures (Figure 2).

Keratinocytes treated with Au@GeMoTi (Figure 6a) maintained a viability higher than 70% (the lowest value established by ISO 10993-57 to consider the material as non-cytotoxic)[67] at all concentrations tested. However, the subcytotoxic Au@GeMoTi concentration was 200 μм for mMSCs and U251MG, while 150 μм was obtained in macrophages and fibroblast cultures. These subcytotoxic concentrations were much higher than the MIC and MBC values obtained for *E. coli*, thus highlighting its potential use as an antibiotic-like agent. Interestingly, Au@PMo nanostructures (Figure 6b) showed high cytocompatibility for all of the five cell lines studied at all concentrations tested, exerting subcytotoxic concentrations higher than 200 μм. In turn, Au@PW nanoparticles (Figure 6c) exerted different subcytotoxic concentrations in the cell lines inspected, though cell viability was higher than 70% at the lowest concentration assayed (100 μм). Finally, Au@PWTi can be considered cytotoxic to the cell types tested at concentrations lower than or equal to 150 μм (Figure 6d). It has been previously reported that the concentrations needed to eradicate bacteria using peptide-based polymer-POM nanocomposites and POM-functionalized AgNPs exerted neither cytotoxicity nor morphological changes toward HeLa and human PC3 epithelial cells, respectively.[52,57] POTs also exerted low cytotoxic effects at MIC and MBC values in HEK-293T and TZM-bl cells,[24] as well as in human dermal fibroblasts.[56]

3. Conclusion

This study demonstrates the relevance of polyoxometalate (POM)-stabilized gold nanoparticles (Au@POM) as antibiotic-like agents and the key relevance of capping POM ligands
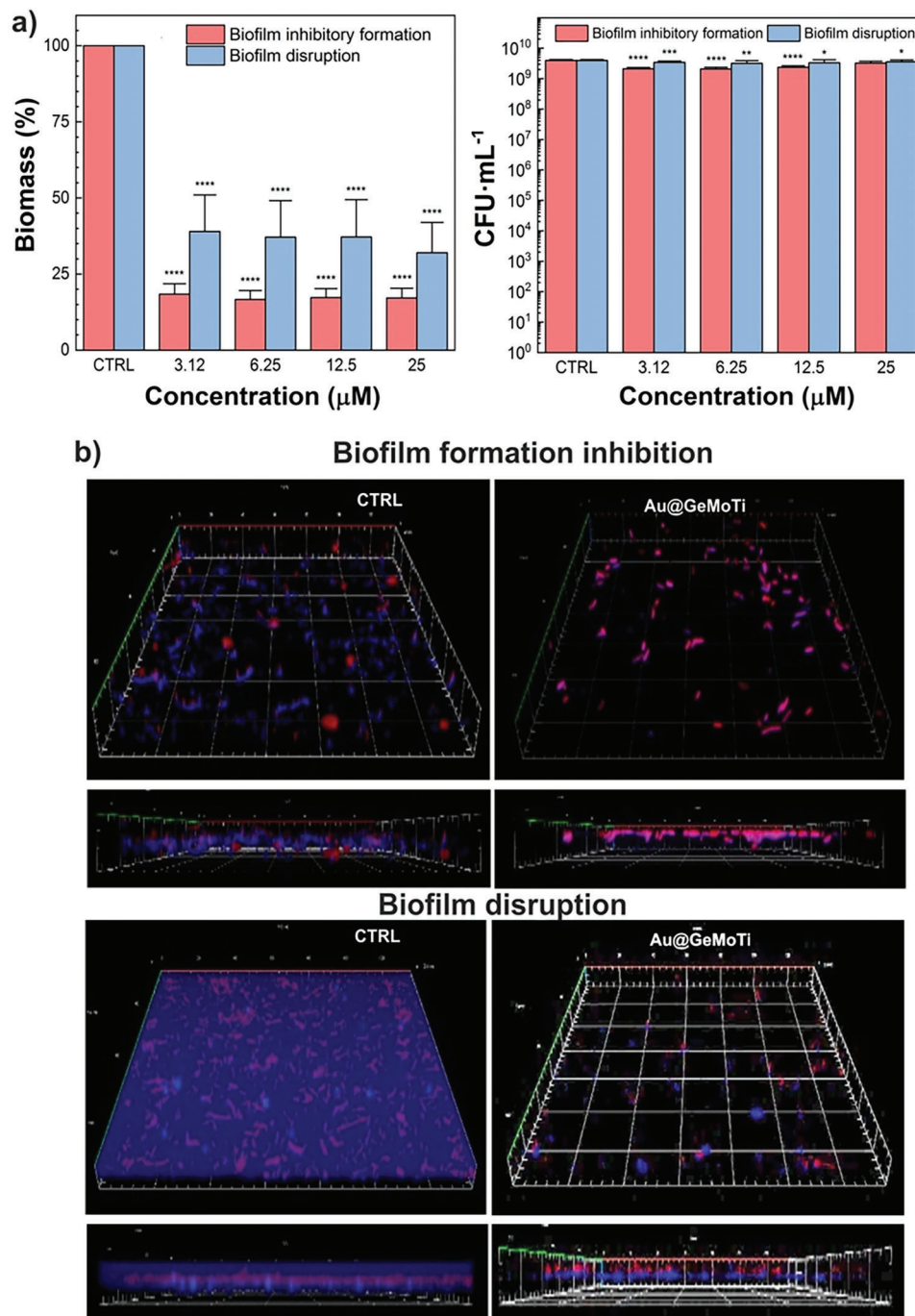
ADVANCED
SCIENCE NEWS

www.advancedsciencenews.com

NANO · MICRO
small
www.small-journal.com

Figure 5. Effect on *E. coli* biofilms of the Au@GeMoTi treatment: inhibition of biofilm formation (red) and disruption of preformed mature biofilm (blue). For each condition, the following experiments are depicted: a) the biofilm formation assay (biomass %) and the bacteria quantification (CFU mL^{-1}); and b) confocal laser scanning microscopies (upper image, bacterial growth at the bottom of the well; lower image, Calcofluor stain of formed biofilms. Color code: bacteria, red; biofilm stain, blue). Data are expressed as mean ± SD of at least three independent experiments performed in triplicate. Statistically significant differences between control and treated samples: $^{*}p < 0.05$; $^{**}p < 0.01$; $^{***}p < 0.001$; and $^{****}p < 0.0001$.

and Au° cores in such context. The bactericidal ability of hybrid Au@POM nanostructures has been successfully demonstrated in a Gram-negative bacteria model (*E. coli*). The Gram-positive bacteria model (*S. aureus*) was significantly less sensitive to Au@POM treatment, probably owing to differences in

the cell wall and outer membrane. The bactericidal effect was particularly remarkable for Au@GeMoTi based on the novel $[Ti_2(HGeMo_7O_{28})_2]^{10-}$ cluster, which represents just the fourth example in the literature of a water-soluble Ti^{IV}-containing polyoxomolybdate, and among them, the first sandwich-type

ADVANCED
SCIENCE NEWS
www.advancedsciencenews.com
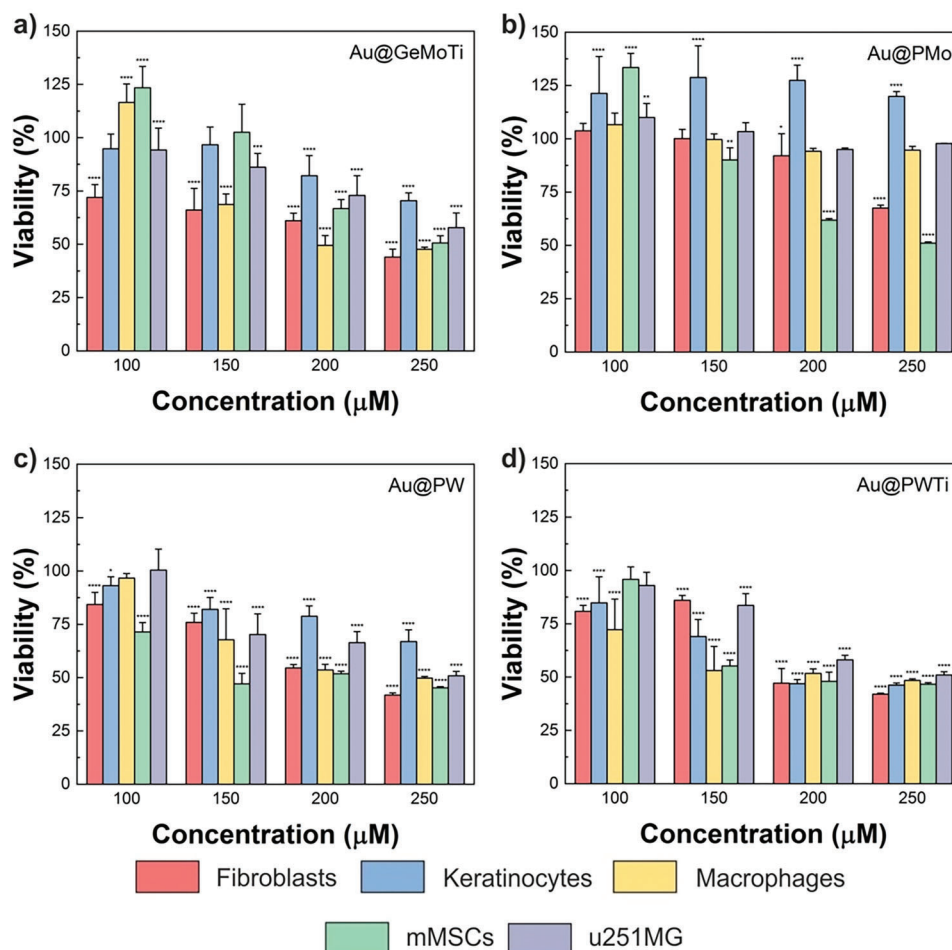
NANO · MICRO
small
www.small-journal.com

Figure 6. Cell viability after treatment with a) Au@GeMoTi, b) Au@PMo, c) Au@PW, and d) Au@PWTi for 24 h on the five cell lines assayed. Control sample (untreated cells) = 100% viability. At least three experiments in triplicate were developed to represent mean ± SD. Statistically significant differences between control and treated samples: $^*p < 0.05$; $^{**}p < 0.01$; $^{***}p < 0.001$; and $^{****}p < 0.0001$.

structure with heteroatoms in the high-oxidation state. The performance of Au@GeMoTi against *E. coli* was found to be 2 orders of magnitude higher than those of the three other Au@POM nanohybrids tested in this work, all of them bearing α-Keggin type reference clusters. Our studies demonstrate that the main bactericidal mechanism displayed by our Au@POM nanoparticles is mediated by cell membrane damage as the bacteria morphology, changes in the membrane polarization, and release of nucleic acids confirm. Moreover, the antibiofilm ability of Au@GeMoTi has also been assessed in both biofilm formation inhibition and preformed biofilm disruption experiments, as well as the reduced cytotoxicity of our Au@POM nanostructures to mammalian cells.

The search for novel antimicrobial approaches to eradicate bacteria without damaging mammalian cells is of paramount importance for future pharmacological strategies against infections. A detailed understanding of the antimicrobial mechanism is key to establishing fundamental principles to design and synthesize antibiotic-like smart nanomaterials. We have shown that the antibiotic-like materials in this work display multiple mechanisms of antimicrobial action and, consequently,

the chances for the bacteria to acquire resistance genes are reduced.

4. Experimental Section

The most important aspects regarding the synthetic procedures, experimental protocols, and techniques used in this work are described below. Further details on materials and methods and associated references are available in the Supporting Information.

Synthesis of $Na_{10}[Ti_2(HGeMo_7O_{28})_2]\cdot34H_2O$ (GeMoTi): The following reagents were successively added to an aqueous 0.5 M NaOAc/HOAc buffer solution (40 mL) under vigorous stirring: GeO_2 (0.093 g, 0.89 mmol), $Na_2MoO_4\cdot2H_2O$ (1.936 g, 8.00 mmol), and $(TiO)SO_4$ hydrate (0.313, 1.96 mmol). The resulting reaction mixture was heated to 90 °C for 1 h, allowed to cool down to room temperature, and filtered to remove any solid material. The yellow filtrate was kept in an open vessel and left to slowly evaporate the remaining solvent at room temperature. Pale-yellow blocks of GeMoTi suitable for single-crystal XRD were isolated when the filtrate was concentrated to ≈15 mL (yield: 0.90 g, 61% based on Ge).

FT-IR (KBr pellet): $\nu = 939$ (m), 934 (m), 926 (m), 901 (s), 841 (m), 764 (s), 741 (s), 725 (s), 671 (br), 600 (versus), and 496 (s) cm^{-1} for the

POM cluster. Anal. calcd for $H_{70}Ge_2Mo_{14}Na_{10}O_{90}Ti_2$ (3324.60 g mol^{-1}): Ge 4.37, Na 6.92, Ti 2.88; found: Ge 4.49, Na 7.18, Ti 2.71. TGA/DTA: Dehydration was observed as two overlapping endothermic mass losses below 375 °C (calcd for 34H_2O: 18.4; found: 19.2%) and final residue obtained at 410 °C after an exothermic process (calcd for $Ge_2Mo_{14}Na_{10}O_{55}Ti_2$: 81,0; found: 80,8%). Crystal data: monoclinic $P2_1/c$, a = 15.5053(2), b = 14.73930(10), c = 18.5897(2) Å, β = 108.1660(10) deg, V = 4036.68(8) Å^3, T = 100(2) K, Z = 2, ρ_{calcd} = 2.735 g cm^{-3}, μ = 3.201 mm^{-1}, 30 034 reflections collected, 7304 unique (R_{int} = 0.0368), 6671 observed [$I > 2\sigma(I)$], 661 parameters / 42 restraints, $R(F)$ = 0.0247 [$I > 2\sigma(I)$], $wR(F^2)$ = 0.0584 (all data), GoF 1.079, max/min e densities 0.538/−0.891 e Å^{-3}; CCDC-2251020 contains the supplementary crystallographic data for this paper, which can be obtained free of charge from the Cambridge Crystallographic Data Centre via www.ccdc.cam.ac.uk/data_request/cif. PXRD (pattern matching): monoclinic $P2_1/c$, a = 15.5308(6), b = 14.7855(6), c = 18.6871(9) Å, β = 108.145(2) deg, 11 parameters, R_p = 5.20, R_{wp} = 7.18, R_{exp} = 3.20, χ^2 = 5.03.

Preparation of Au@POM Nanoparticles: Stock 2.0 mм solutions of $HAuCl_4$ and the four selected POM photocatalysts: GeMoTi, PMo ($H_3PMo_{12}O_{40}$), PW ($H_3PW_{12}O_{40}$), and PWTi ($K_7[PTi_2W_{10}O_{40}]$) were first prepared in deionized water. Then, as previously described,[48] 10 mL of the $HAuCl_4$ solution was mixed with an equal volume of the corresponding POM solution, and, upon deoxygenation with a N_2 stream for 5 min, the resulting mixture was irradiated under mild stirring with UV light provided by a LED lamp placed at 25 mm over the center of the reaction vessel (Thorlabs M365LP1 – 365 nm, 1350 mW). Natural PVA was added to the vessel as a 2 cm long filament (2.85 mm diameter) immediately before turning the UV light on and the reaction mixture was irradiated for 2 h to induce the in situ formation of Au@POM nanoparticles. The final, burgundy-colored Au@POM dispersions were transferred to clean vials for storage at 4 °C until being used for antimicrobial studies as-synthesized without any further purification. The formation of hybrid Au@POM nanostructures was monitored through UV–vis spectroscopy and confirmed by TEM. The nanoparticle diameters were determined from statistical analysis of TEM images.

Au@POM Antimicrobial Activity: Minimum inhibitory (MIC) and bactericidal (MBC) Au@POM concentrations were tested in two bacteria cultures, *E. coli* and *S. aureus*. Both strains were grown overnight in TSB at 37 °C under shaking (150 rpm), reaching stationary phase growth (10^8– 10^9 CFU mL^{-1}). These overnight cultures were diluted (10^5 CFU mL^{-1}) in TSB and subsequently exposed to different final concentrations (0– 500 μм) of Au@PWTi, Au@PMo, Au@GeMoTi, and Au@PW for 24 h at 37 °C under shaking (150 rpm). Then, the broth microdilution method[68] was carried out to determine viable bacteria. As a positive control, untreated bacteria were included, as well as an assay performed on the selected bacteria using the highest concentration of PVA and water (without the antimicrobials agents) to corroborate that the Au@POM dispersion media did not cause any antimicrobial action by themselves.

To evaluate the influence of UV light on the Au@POM bactericidal effect, samples were irradiated using a 365 nm UV LED lamp (Thorlabs M365LP1 – 365 nm, 1350 mW) for 30 min at a total energy of 110 J cm^{-2}. Irradiated-Au@POM samples were subsequently added to the corresponding bacterial suspension (10^5 CFU mL^{-1}) at different final concentrations (0–500 μм) for 24 h at 37 °C under shaking (150 rpm). Then, the microdilution assay was developed as described above.

Evaluation of Au@POM Antimicrobial Mechanisms: The bacteria morphology before and after Au@POM treatment (either irradiated or non-irradiated) was analyzed by SEM as previously reported.[69] Briefly, incubated samples were spin-dried and washed twice in 0.1 м PBS. Bacteria were then fixed in 2.5% glutaraldehyde, and after 90 min, filtered and dehydrated twice in a series of 30–100% ethanol solutions for 15 min. Finally, air-dried samples were covered with Pt (10 nm) to acquire SEM micrographs. To study the Au@POM ability for modulating cell hyperpolarization,[26] *E. coli* (10^5 CFU mL^{-1}) was treated with such nanoparticles at MIC and MBC and incubated for 2 and 24 h at 37 °C. Control groups (non-treated bacteria) were also analyzed. After incubation, the bacteria were collected and resuspended in PBS. To evaluate changes in the membrane potential, 5 μL of DilC1(5) were added to the resuspended

bacteria, which were then incubated for 15 min (37 °C, 5% CO_2) before being analyzed by flow cytometry. To corroborate whether the Au@POM bactericidal effect is mediated by cell wall disruption mechanisms,[51] *E. coli* (10^5 CFU mL^{-1}) was incubated with Au@POM nanoparticles at MIC and MBC for 2 and 4 h in TSB at 37 °C. The resulting bacterial suspensions were centrifuged (3500 rpm, 5 min) and nucleic acids present in the supernatants were quantified by a fluorescence technique (Qubit ss-DNA Assay). For propidium iodide (PI) staining, *E. coli* was exposed to Au@POM nanoparticles at the MIC value for 24 h in TSB at 27 °C. Subsequently, 2.5 μL of a 1 mg mL^{-1} PI solution was added. The cells were then incubated in the dark at room temperature for 15 min and subjected to analysis using flow cytometry.

Au@POM Effect on E. coli Biofilms: The studies carried out to evaluate biofilm formation inhibition or eradication were performed using Au@GeMoTi samples only. For the biofilm formation,[70] *E. coli* was grown overnight in TSB until reaching the stationary growth phase. At this point, the bacteria were adjusted to 10^7 CFU mL^{-1} and the effect of the treatment with Au@GeMoTi and irradiated-Au@GeMoTi samples on *E. coli* biofilms were studied following two different methodologies:

1) In the first approach, the Au@GeMoTi effect on the biofilm disruption was studied. Briefly, the bacteria at 10^7 CFU mL^{-1} were incubated in 60 mm Petri dishes at 37 °C for 16 h without shaking. Then, the resulting biofilms were washed twice with PBS and different concentrations of Au@GeMoTi or irradiated-Au@GeMoTi samples (3.12–31.25 μм) were added to the preformed mature biofilms before incubation for 24 h at 37 °C without shaking.

2) In the second methodology, the Au@GeMoTi effect during the biofilm formation was assessed. Briefly, Au@GeMoTi or irradiated-Au@GeMoTi samples at different concentrations (3.12–31.25 μм) were added to bacterial suspensions (10^7 CFU mL^{-1}) and incubated in 60 mm Petri dishes for 24 h at 37 °C without shaking.

After incubation, planktonic cells were removed by washing them twice with PBS and three different methodologies were carried out to study the effect on the final *E. coli* biofilms:

1) For the crystal violet (CV) staining method, the biofilms were washed twice with PBS and 0.1% (w/v) CV was added to the biofilm matrix before being incubated for 15 min at room temperature. After removing the excess CV by washing twice with PBS, the fixed CV was released using an acetone-alcohol (20:80, v/v) solution. The biofilms were then quantified by measuring the absorbance at 590 nm with a microplate reader. The results were expressed as a percentage of biomass formation.[71]

2) For the bacteria quantification, the biofilms were harvested and disrupted. Then, the detached bacteria were quantified following the conventional serial microdilution method described above.

3) For confocal microscopy, the biofilms were fixed with 4% paraformaldehyde in PBS, incubated (45 min), washed, and stained with the nuclear fluorescent dye Syto 59 for 30 min. The stained biofilms were then washed and incubated for 30 min in the dark with 0.025% Calcofluor white M2R. Finally, the samples were mounted in Mowiol mounting medium to be further visualized under confocal microscopy.[72]

Au@POM Cytocompatibility: Human dermal fibroblasts, THP1 human monocytes, human epidermal keratinocytes, U251MG cells, and mMSCs were employed to determine the possible cytotoxic effects of Au@POM nanoparticles in different mammalian cells. The cell culture methodology and the viability assays carried out for this purpose are detailed in Supporting Information.

Statistical Analyses: All results were expressed as the mean ± SD. The statistical data analyses were executed using the Prism 7 software (Version 7.04, GraphPad Software Inc., US). A one-way analysis of variance (ANOVA) set for multiple comparisons with a Dunnett's post-test and *t*-test analysis was used. Statistically significant differences were considered when $p \leq 0.05$.

Supporting Information

Supporting Information is available from the Wiley Online Library or from the author.

Acknowledgements

Conflict of Interest

The authors declare no conflict of interest.

Author Contributions

The manuscript was written through the contributions of all authors. All authors have given approval to the final version of the manuscript.

Data Availability Statement

The data that support the findings of this study are available from the corresponding author upon reasonable request.

[1] S.-S. Wang, G.-Y. Yang, *Chem. Rev.* **2015**, *115*, 4893.
[2] D. Cheng, K. Li, H. Zang, J. Chen, *Energy Environ. Mater.* **2023**, *6*, e12341.
[3] P. Song, T. Wang, *ACS Sens.* **2022**, *7*, 3634.
[4] J. Zhong, J. Pérez-Ramírez, N. Yan, *Green Chem.* **2021**, *23*, 18.
[5] L. Yang, J. Lei, J.-M. Fan, R.-M. Yuan, M.-S. Zheng, J.-J. Chen, Q.-F. Dong, *Adv. Mater.* **2021**, *33*, 2005019.
[6] J.-H. Kruse, M. Langer, I. Romanenko, I. Trentin, D. Hernández-Castillo, L. González, F. H. Schacher, C. Streb, *Adv. Funct. Mater.* **2022**, *32*, 2208428.
[7] S. G. Mitchell, J. M. De La Fuente, *J. Mater. Chem.* **2012**, *22*, 18091.
[8] U. Jameel, M. Zhu, X. Chen, Z. Tong, *J. Mater. Sci.* **2016**, *51*, 2181.
[9] M. Lafuente, I. Pellejero, A. Clemente, M. A. Urbiztondo, R. Mallada, S. Reinoso, M. P. Pina, L. M. Gandía, *ACS Appl. Mater. Interfaces* **2020**, *12*, 36458.
[10] M. Arefian, M. Mirzaei, H. Eshtiagh-Hosseini, A. Frontera, *Dalton Trans.* **2017**, *46*, 6812.
[11] A. Bijelic, M. Aureliano, A. Rompel, *Chem. Commun.* **2018**, *54*, 1153.
[12] H. Stephan, M. Kubeil, F. Emmerling, C. E. Müller, *Eur. J. Inorg. Chem.* **2013**, *2013*, 1585.
[13] A. Bijelic, M. Aureliano, A. Rompel, *Angew. Chem., Int. Ed.* **2019**, *58*, 2980.
[14] L. S. Van Rompuy, T. N. Parac-Vogt, *Curr. Opin. Biotechnol.* **2019**, *58*, 92.
[15] A. Bijelic, A. Rompel, *Coord. Chem. Rev.* **2015**, *299*, 22.
[16] C. Molitor, A. Bijelic, A. Rompel, *Chem. Commun.* **2016**, *52*, 12286.
[17] H. K. Daima, P. R. Selvakannan, R. Shukla, S. K. Bhargava, V. Bansal, *PLoS One* **2013**, *8*, e79676.
[18] S. Norrby, C. Nord, R. Finch, *Lancet Infect. Dis.* **2005**, *5*, 115.
[19] M. Leeb, *Nature* **2004**, *431*, 892.
[20] F. Nederberg, Y. Zhang, J. P. K. Tan, K. Xu, H. Wang, C. Yang, S. Gao, X. D. Guo, K. Fukushima, L. Li, J. L. Hedrick, Y.-Y. Yang, *Nat. Chem.* **2011**, *3*, 409.
[21] N. Fukuda, T. Yamase, *Biol. Pharm. Bull.* **1997**, *20*, 927.
[22] M. Inoue, K. Segawa, S. Matsunaga, N. Matsumoto, M. Oda, T. Yamase, *J. Inorg. Biochem.* **2005**, *99*, 1023.
[23] E. Bae, J. W. Lee, B. H. Hwang, J. Yeo, J. Yoon, H. J. Cha, W. Choi, *Chemosphere* **2008**, *72*, 174.
[24] A. G. Enderle, I. Franco-Castillo, E. Atrián-Blasco, R. Martín-Rapún, L. Lizarraga, M. J. Culzoni, M. Bollini, J. M. De La Fuente, F. Silva, C. Streb, S. G. Mitchell, *ACS Appl. Polym. Mater.* **2022**, *4*, 4144.
[25] Y. Zhang, Y. Pi, Y. Hua, J. Xie, C. Wang, K. Guo, Z. Zhao, Y. Yong, *Theranostics* **2020**, *10*, 10031.
[26] K. Chen, Q. Yu, Y. Liu, P. Yin, *J. Inorg. Biochem.* **2021**, *220*, 111463.
[27] O. Oms, A. Dolbecq, P. Mialane, *Chem. Soc. Rev.* **2012**, *41*, 7497.
[28] J.-W. Zhao, Y.-Z. Li, L.-J. Chen, G.-Y. Yang, *Chem. Commun.* **2016**, *52*, 4418.
[29] J.-C. Liu, J.-W. Zhao, C. Streb, Y.-F. Song, *Coord. Chem. Rev.* **2022**, *471*, 214734.
[30] K. Nomiya, Y. Sakai, S. Matsunaga, *Eur. J. Inorg. Chem.* **2011**, *2011*, 179.
[31] B. Chakraborty, I. A. Weinstock, *Coord. Chem. Rev.* **2019**, *382*, 85.
[32] P. J. Domaille, W. H. Knoth, *Inorg. Chem.* **1983**, *22*, 818.
[33] K. Dan, T. Yamase, *Biomed. Pharmacother.* **2006**, *60*, 169.
[34] Y.-F. Qi, H. Zhang, J. Wang, Y. Jiang, J. Li, Y. Yuan, S. Zhang, K. Xu, Y. Li, J. Li, J. Niu, E. Wang, *Antiviral Res.* **2012**, *93*, 118.
[35] S. Shigeta, S. Mori, E. Kodama, J. Kodama, K. Takahashi, T. Yamase, *Antiviral Res.* **2003**, *58*, 265.
[36] M. Inoue, T. Suzuki, Y. Fujita, M. Oda, N. Matsumoto, J. Iijima, T. Yamase, *Biomed. Pharmacother.* **2006**, *60*, 220.
[37] M. Inoue, T. Suzuki, Y. Fujita, M. Oda, N. Matsumoto, T. Yamase, *J. Inorg. Biochem.* **2006**, *100*, 1225.
[38] C. Li, A. Jimbo, K. Yamaguchi, K. Suzuki, *Chem. Sci.* **2021**, *12*, 1240.
[39] F. Li, L. Xu, *Dalton Trans.* **2011**, *40*, 4024.
[40] M. Xu, T. Wang, F. Li, W. Xu, Y. Zheng, L. Xu, *Chem. Commun.* **2020**, *56*, 1097.
[41] W. Xu, M. Xu, Y. Zheng, X. Wang, F. Li, L. Xu, *Inorg. Chem. Front.* **2020**, *7*, 3667.
[42] L. Li, Q. Shen, G. Xue, H. Xu, H. Hu, F. Feng, J. Wang, *Dalton Trans.* **2008**, *2008*, 5698.

ADVANCED
SCIENCE NEWS

www.advancedsciencenews.com

NANO · MICRO

small

www.small-journal.com

[43] H. Xu, L. Li, B. Liu, G. Xue, H. Hu, F. Fu, J. Wang, *Inorg. Chem.* **2009**, *48*, 10275.

[44] Y. Yang, L. Xu, G. Gao, F. Li, Y. Qiu, X. Qu, H. Liu, *Eur. J. Inorg. Chem.* **2007**, *2007*, 2500.

[45] S. Li, J. Zhao, P. Ma, J. Du, J. Niu, J. Wang, *Inorg. Chem.* **2009**, *48*, 9819.

[46] I. D. Brown, D. Altermatt, *Acta Crystallogr.* **1985**, *41*, 244.

[47] A. Troupis, A. Hiskia, E. Papaconstantinou, *Angew. Chem., Int. Ed.* **2002**, *41*, 1911.

[48] I. Pellejero, A. Clemente, S. Reinoso, A. Cornejo, A. Navajas, J. J. Vesperinas, M. A. Urbiztondo, L. M. Gandía, *Catal. Today* **2022**, *383*, 164.

[49] K. H. Wu, P. Y. Yu, C. C. Yang, G. P. Wang, C. M. Chao, *Polym. Degrad. Stab.* **2009**, *94*, 1411.

[50] C. J. Moll, K. Meister, J. Kirschner, H. J. Bakker, *J. Phys. Chem. B* **2018**, *122*, 10722.

[51] M. Zhao, Y. Fang, L. Ma, X. Zhu, L. Jiang, M. Li, Q. Han, *J. Inorg. Biochem.* **2020**, *210*, 111131.

[52] L. P. Datta, R. Mukherjee, S. Biswas, T. K. Das, *Langmuir* **2017**, *33*, 14195.

[53] R. Kumar, S. K. Shukla, M. Pandey, A. Pandey, A. Pathak, A. Dikshit, *Cogent Chem.* **2016**, *2*, 1192522.

[54] A. Scala, A. Piperno, A. Hada, S. Astilean, A. Vulpoi, G. Ginestra, A. Marino, A. Nostro, V. Zammuto, C. Gugliandolo, *Polymers* **2019**, *11*, 1157.

[55] M. Moghayedi, E. K. Goharshadi, K. Ghazvini, H. Ahmadzadeh, R. Ludwig, M. Namayandeh-Jorabchi, *Mater. Chem. Phys.* **2017**, *188*, 58.

[56] C. Zhang, M. Zhao, H. Zou, X. Zhang, R. Sheng, Y. Zhang, B. Zhang, C. Li, Y. Qi, *J. Inorg. Biochem.* **2020**, *212*, 111212.

[57] H. K. Daima, P. R. Selvakannan, A. E. Kandjani, R. Shukla, S. K. Bhargava, V. Bansal, *Nanoscale* **2014**, *6*, 758.

[58] S. Borse, S. Joshi, *Adv. Chem. Lett.* **2013**, *1*, 15.

[59] D. N. Williams, S. H. Ehrman, T. R. Pulliam Holoman, *J. Nanobiotechnol.* **2006**, *4*, 3.

[60] M. Paesa, C. Remirez De Ganuza, T. Alejo, C. Yus, S. Irusta, M. Arruebo, V. Sebastian, G. Mendoza, *J. Colloid Interface Sci.* **2023**, *633*, 786.

[61] J. M. Maestre, X. Lopez, C. Bo, J.-M. Poblet, N. Casañ-Pastor, N. Casañ-Pastor, *J. Am. Chem. Soc.* **2001**, *123*, 3749.

[62] S. Tomane, E. López-Maya, S. Boujday, V. Humblot, J. Marrot, N. Rabasso, J. Castells-Gil, C. Sicard, A. Dolbecq, P. Mialane, A. Vallée, *Nanoscale Adv* **2019**, *1*, 3400.

[63] J. Gu, L. Zhang, X. Yuan, Y.-G. Chen, X. Gao, D. Li, *Bioinorg. Chem. Appl.* **2018**, *2018*, 9342326.

[64] J. Li, Z. Chen, M. Zhou, J. Jing, W. Li, Y. Wang, L. Wu, L. Wang, Y. Wang, M. Lee, *Angew. Chem., Int. Ed.* **2016**, *55*, 2592.

[65] X. Liu, Z. Ma, J. Nie, J. Fang, W. Li, *Biomacromolecules* **2022**, *23*, 1009.

[66] P. Raj, A. Singh, A. Singh, N. Singh, *ACS Sustainable Chem. Eng.* **2017**, *5*, 6070.

[67] ISO – ISO 10993–5:2009 – Biological evaluation of medical devices — Part 5: Tests for in vitro cytotoxicity, https://www.iso.org/standard/36406.html, (accessed: March, **2023**).

[68] CLSI, *Methods for Dilution Antimicrobial Susceptibility Tests for Bacteria That Grow Aerobically*, 11th ed., CLSI standard M07, Clinical and Laboratory Standards Institute, Wayne PA, USA **2018**.

[69] G. Mendoza, A. Regiel-Futyra, V. Andreu, V. Sebastián, A. Kyziol, G. Stochel, M. Arruebo, *ACS Appl. Mater. Interfaces* **2017**, *9*, 17693.

[70] S. Garcia-Salinas, E. Gámez, G. Landa, M. Arruebo, S. Irusta, G. Mendoza, *ACS Appl. Mater. Interfaces* **2020**, *12*, 51302.

[71] J. H. Merritt, D. E. Kadouri, G. A. O'Toole, *Curr. Protoc. Microbiol.* **2006**, *00*, 17.

[72] K. Ranjith, J. Ramchiary, J. S. S. Prakash, K. Arunasri, S. Sharma, S. Shivaji, *Front. Microbiol.* **2019**, *10*, 1308.